

Structural and Functional Characterization of Luminescent Silver–Protein Nanobioconjugates

S. Shankara Narayanan and Samir Kumar Pal*

Unit for Nano Science & Technology, Department of Chemical, Biological & Macromolecular Sciences, S. N. Bose National Centre for Basic Sciences, Block JD, Sector III, Salt Lake, Kolkata 700 098, India

Received: October 15, 2007; In Final Form: January 18, 2008

In this contribution, we report synthesis of luminescent Ag nanoclusters (NCs, 1 nm average diameter) directly conjugated to an enzyme, bovine pancreatic α -chymotrypsin (CHT). The structural characterization of Ag–CHT nanobioconjugates was done using steady-state UV–vis absorption/photoluminescence spectroscopy and high-resolution transmission electron microscopy. By use of the spherical jellium model, the emission energy of CHT-conjugated Ag NCs was correlated with the number of atoms in the cluster and was found to be almost consistent with the experimental result. To establish the conformational changes of the enzyme before and after the conjugation of Ag NCs, circular dichroism studies were performed. The functional integrity of the enzyme conjugated to Ag NCs was investigated by monitoring the enzymatic activity of Ag–CHT conjugates by using UV–vis absorption spectroscopy and compared with the unbound enzyme under similar experimental conditions. To confirm the conjugation of Ag NCs to CHT, we carried out the Förster resonance energy transfer studies using a fluorescent probe, 4-nitrophenyl anthranilate, known to bind at the enzymatic active site of CHT, as the donor and Ag-NC-bound CHT as the acceptor. The attachment of Ag NCs to an enzyme with its structural and functional integrity may have an impact in the future research on nanobio interfaces.

Introduction

Biological systems form sophisticated mesoscopic and macroscopic structures with tremendous control over the placement of nanoscopic building blocks within extended architectures. Both biotechnology and materials science meet at the same length scale because biomolecular components have typical size dimensions in the range of about 2–100 nm. To exploit and to utilize the concepts administered in natural nanometer-scale systems, the development of nanochemistry is crucial. In this regard, bioconjugate synthesis of nanoparticles using biological macromolecules^{1,2} has recently aroused great interest due to the broad range of applications of such hybrid materials from life sciences to materials and nanosciences. The motivation is based on the unique properties of nanoparticles possessing strongly size-dependent optical, electrical, magnetic, and electrochemical properties combined with the perfect binding and biochemical functionality of biomacromolecules. The synthesis of metal nanoparticles has, in particular, received considerable attention,³ and their potential applications in catalysis,^{4,5} single electron tunneling,⁶ nonlinear optical devices,⁷ and DNA sequencing⁸ have been demonstrated. Examples of biotemplate synthesis of metal nanoparticles include the binding of metal ions to surface-layer proteins,⁹ DNA,¹⁰ virus protein cages,¹¹ or ordered protein assemblies¹² to initiate sites of nucleation for nanoparticle growth and the synthesis of metallic nanocrystals through the use of amino acids as a capping and reducing agents in an aqueous medium.¹³

Similar to larger metal nanoparticles, synthesis of metal nanoclusters (NCs), which consists of small numbers of metal atoms, has also received considerable attention in recent years.

Their strong, robust, discrete, size-dependent emission makes them ideal fluorophores for single-molecule spectroscopic studies. The binding of proteins to metal clusters is more or less irreversible. Most of the proteins retain their biological activities, at least in part. This property makes NCs highly useful as transducers. The metal NCs, which have sizes comparable to the Fermi wavelength of an electron, exhibit moleculelike behavior including discrete electronic states and size-dependent fluorescence^{14,15} due to quantum size effect. Their transition energies have been found to scale with the inverse cluster radius based on the spherical jellium model, valid for metals with free electrons such as gold and silver.¹⁶ This model predicts that the emission energy of metallic NCs is a power law of the number of atoms in the NC with no adjustable parameters by the simple scaling relation of $E_{\text{fermi}}/N^{1/3}$ in which E_{fermi} is the Fermi energy of bulk metal and N is the number of atoms in the NC. It has been successfully applied to small gold NCs,¹⁷ describing accurately the size-dependent electronic structure and relative electronic transitions of the small clusters. To the best of our knowledge, the jellium model has not yet been applied to silver nanocrystals to correlate their emission energy with the number of atoms, which is one of the motives of our present studies.

In the present work, we have synthesized luminescent silver NCs of 1 nm average diameter using an enzyme, bovine pancreatic α -chymotrypsin (CHT). We obtain a well-dispersed, protein-conjugated silver NC that remained stable indefinitely in solution without any aggregation or deterioration of the spectral properties. The structural characterization of CHT-conjugated Ag NCs was done using steady-state UV–vis absorption/photoluminescence (PL) spectroscopy and high-resolution transmission electron microscopy (HRTEM). A comparative study on the enzymatic activity of the nanobio-

* To whom correspondence should be addressed. E-mail: skpal@bose.res.in. Fax: 91 33 2335 3477.

conjugates with the unbound enzyme, under similar experimental conditions, was also done. Picosecond-resolved Förster resonance energy transfer (FRET) from a fluorescent probe at the enzymatic active site to the Ag NC in the nanobioconjugates reveals the possible location of the metal cluster in CHT. Our detail structural and functional characterization of the nanobioconjugates may find its application in the field of biofunctionalization of metal NC.

Materials and Methods

Sample Preparation. Silver nitrate (AgNO_3 , >99.9%), sodium borohydride (NaBH_4 , >99.9%), CHT, 4-nitrophenyl anthranilate (NPA), and Ala-Ala-Phe 7-amido-4-methyl coumarin (AAF-AMC) were obtained from Sigma Aldrich. The chemicals and the proteins are of highest commercially available purity and were used as received. All aqueous solutions were prepared using double distilled water from a Millipore system and then degassed by bubbling with dry argon gas for 1 h to well control the growth of NCs as pointed out by Wilcoxon et al.¹⁸ Since sodium borohydride, catalyzed by metallic ions, can react directly with water to form hydrogen,¹⁹ freshly prepared aqueous solutions of NaBH_4 were used in the experiment. The synthesis of CHT-conjugated Ag NCs was carried out, following the method of Burt et al.²⁰ by chemical reduction in the aqueous solution using NaBH_4 as a reducing agent at ambient conditions. The typical procedure for the synthesis of conjugated Ag NCs is as follows: 10 mL of 100 μM CHT aqueous solution was prepared and dialyzed exhaustively against Millipore water at 4 °C. This was carefully degassed with argon gas for 30 min. A freshly prepared AgNO_3 solution (100 μL of 100 mM) was then added to the above protein solution with vigorous stirring under an argon blanket. A degassed aqueous NaBH_4 solution (1 M) was then added to the above solution under vigorous stirring. The final molar ratio of $\text{BH}_4^-:\text{Ag}^+$ in the aqueous solution was maintained at 10:1. The reaction was allowed to proceed for 3 h, and the final solution was dialyzed against water exhaustively to remove any excess of salts and NaBH_4 left in the solution. The final dialyzed solution was collected and stored at 4 °C prior to analysis. The details of the experimental methodology including steady-state and time-resolved measurements can be obtained from the Supporting information.

Results and Discussion

Figure 1a presents the HRTEM image of dialyzed sample of Ag–CHT nanobioconjugates at 100 K magnification which reveals a uniform size distribution of small spherical NCs. However, some of the aggregated clusters can also be seen in the TEM image, which are likely to have been formed in the original sample (i.e., NC sample before dialysis) due to the presence of excess of NaBH_4 , which is known to induce aggregation of nanoparticles.²¹ A statistical analysis of ~ 200 small clusters (by hand) yields an average cluster size of ~ 1 nm and a standard deviation of 0.2 nm. The corresponding selected area electron diffraction pattern (SAED) (left of Figure 1b) shows diffuse diffraction rings along with small diffraction spots indicating a very low crystallinity (nearly amorphous) in the sample. Because the diffraction originates from a large number of clusters of very small size (diameter ≈ 1 nm) rather than from a single crystal, diffuse rings are observed in the diffraction pattern.²² The corresponding FFT image (right of Figure 1b) confirms that these NCs assume some crystallinity in their structure. Figure 2a presents the HRTEM image of the undialyzed sample of Ag–CHT conjugates, which reveals particles of larger diameter of ~ 4 –5 nm. The presence of larger

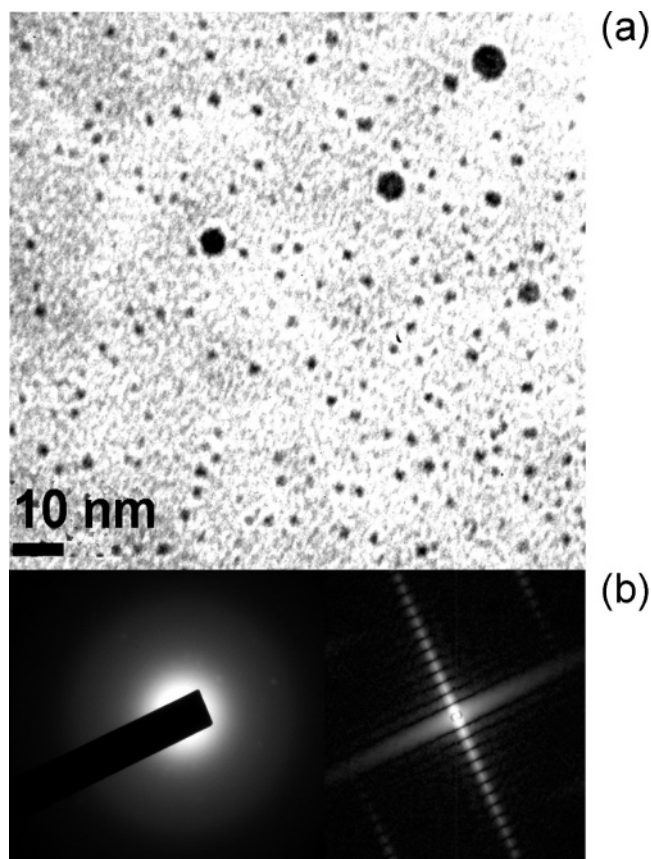


Figure 1. (a) HRTEM of dialyzed Ag–CHT nanobioconjugates. (b) SAED pattern and the corresponding FFT image of dialyzed Ag–CHT nanobioconjugates.

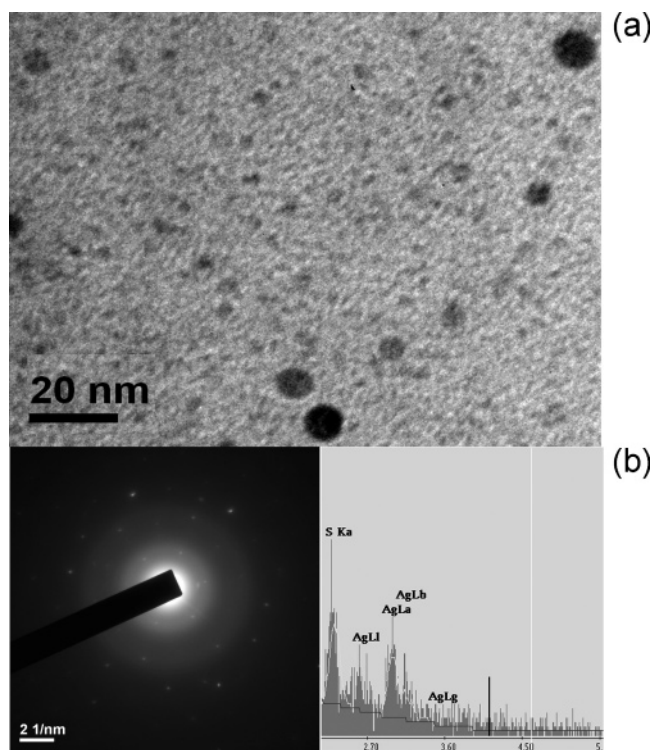


Figure 2. (a) HRTEM of undialyzed Ag–CHT nanobioconjugates. (b) SAED pattern (undialyzed sample) and EDAX spectrum (dialyzed sample) of Ag–CHT nanobioconjugates.

particles in an undialyzed sample as compared to the majority of smaller particles found in a dialyzed sample in TEM image could be attributed to the presence of excess of NaBH_4 in the

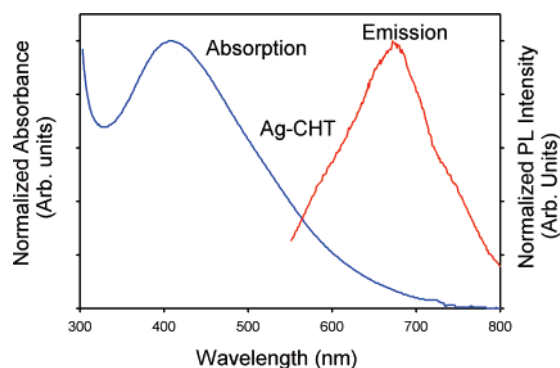


Figure 3. Steady-state UV-vis absorption and PL spectra of Ag-CHT nanobioconjugates (excitation wavelength = 500 nm).

undialyzed sample leading to increase in the pH of the undialyzed solution, which induces aggregation of NCs consistent with a previous study on pH-induced aggregation of dendrimer-protected silver nanoparticles by Zheng et al.²¹ However, this pH-induced flocculation of nanoparticles is reversible if pH is lowered within a period of hours after aggregation/precipitation. The exhaustive dialysis of our NC sample against Millipore water confirmed complete removal of excess of NaBH₄ (leading to lowering in pH). This is borne out by the observation of majority of unaggregated small NCs in the TEM images of dialyzed sample. It has to be noted that the average size of 1 nm Ag NCs obtained in the dialyzed sample, which is confirmed from TEM and absorption studies (see below in the text), cannot be formed from free Ag ions because of unavailability of any stabilizing agent to control their size. Thus in our experimental condition, the possibility of formation of free larger Ag nanoparticles of micrometer size (due to uncontrolled growth) is negligibly small as they are not revealed in the TEM images of dialyzed sample. However, the aggregated nanostructures seen in the undialyzed sample could be attributed to the presence of excess of NaBH₄ in the solution, which induces aggregation of the NCs. The SAED pattern of the undialyzed sample (left of Figure 2b) simultaneously obtained in the TEM measurement showed four distinct diffraction rings corresponding to the interplanar spacing of 2.35, 2.01, 1.18, and 0.91 Å, which were assignable to diffractions from (111), (200), (222), and (420) planes of a face-centered cubic (fcc) crystal structure of silver, respectively (JCPDS, International Center for Diffraction Data, No. 4-783). A typical energy-dispersive X-ray (EDAX) spectrum of the dialyzed Ag-CHT sample is shown in the right of Figure 2b and demonstrates the presence of Ag and S. Although the N peaks are not detected because of its small atomic number, the appearance of S peak indicates that the silver NCs are bound to the protein matrix.

Silver metal is known to have an intense plasmon absorption band in the visible region.²³ Figure 3 shows the UV-vis absorption spectrum of Ag-CHT conjugates, which reveals a surface plasmon band located at 413 nm. On the basis of Mie theory²⁴ and its expanded versions,^{25,26} information concerning silver nanoparticle sizes can be derived from the analysis of this absorption band. The linear optical absorption coefficient, $\sigma(\lambda)$, of a collection of uniform metallic spheres whose dimensions are very small compared to the wavelength of the incident light is well described by Mie scattering theory in the electric dipole approximation and is given by

$$\sigma(\lambda) = \left(\frac{18\pi V \epsilon_m^{3/2}}{\lambda} \right) \frac{\epsilon''(\omega)}{(\epsilon'(\omega) + 2\epsilon_m)^2 + \epsilon''(\omega)^2} \quad (1)$$

where λ is the incident wavelength with a corresponding frequency ω , V is the volume of the spherical particle (i.e., $4\pi r^3/3$), ϵ_m is the dielectric constant of the medium, and $\epsilon'(\omega)$ and $\epsilon''(\omega)$ are the real and the imaginary parts of the dielectric constant of the metal. The absorption coefficient in eq 1 has a maximum value at the surface plasmon resonance (SPR) frequency, when $\epsilon'(\omega) + 2\epsilon_m = 0$, the peak wavelength of the band depending on the dielectric constants of the medium and the metal particles.

The average radius of silver NCs (assumed to be spherical), small compared to the wavelength of light, can be approximately estimated from the resonance optical absorption spectrum as per the Mie scattering formula^{24,27}

$$r_{\text{metal}} = \frac{v_F}{\Delta\omega_{1/2}} = \frac{v_F}{2\pi c_0 \left(\frac{\Delta\lambda}{\lambda_p^2} \right)} \quad (2)$$

where v_F = Fermi velocity (1.39×10^6 m/s for Ag) and $\Delta\omega_{1/2}$ is the full width at half-maximum (FWHM) of the SPR absorption when plotted as a function of angular frequency ω , c_0 is the speed of light in vacuum, λ_p is the wavelength where absorption peak appears, and $\Delta\lambda$ gives the FWHM of the band. The average radius of the NCs calculated using eq 2 is found to be in the range of 1.0–1.4 nm, consistent with the size obtained from the TEM image of the dialyzed sample, and is close to the value obtained recently by Balan et al.²⁸ for silver nanoparticles prepared in tetrahydrofuran.

It has been demonstrated previously²⁹ for spherical NCs that the broadening of the plasmon with decreasing size in the quantum size regime, $d < 3$ nm, in the case of both Au and Ag is rapid and increases the absorbance of both UV and NIR regions relative to the plasmon peak, whose height decreases. It is in fact well established that the surface plasmon bandwidth is inversely proportional to the radius r of the particle for sizes smaller than about 20 nm.^{30,31} The increased broadening with decreasing size enhances both the low- and high-energy absorbance of the smallest clusters, causing the plasmon to be completely damped below a size of $d = 2.2$ nm for Au but still observable at the size of $d = 1.55$ nm for Ag.²⁹ Thus the surface plasmon band obtained in our sample indeed indicates the formation of small size silver NCs. The plasmon band shown in Figure 3 has also been observed previously for silver clusters with a diameter of 1 nm, which have been stabilized for long periods in the presence of appropriate stabilizers³² and have also been observed recently for silver nanoparticles prepared in tetrahydrofuran.²⁸ As opposed to larger metal nanoparticles, a distinctive feature of small NCs is their strong, robust, discrete, size-dependent emission, which arises when the particle size becomes comparable with the Fermi wavelength of an electron (~ 0.5 nm for Ag). For the protein-bound Ag NCs, a prominent fluorescence is observed at ~ 680 nm when excited at 500 nm (Figure 3). The size distribution of these silver nanoclusters was studied by exciting the nanoclusters at various excitation wavelengths (from 475 to 550 nm), which resulted in an insignificant shift in the emission maxima, suggesting a narrow size distribution. Recently, Dickson and co-workers reported near-IR-emitting DNA-encapsulated silver nanoclusters,³³ which exhibited emission peak around 700 nm close to the emission peak obtained in our experiment.

By assumption of a spherical shape and a uniform fcc structure,³⁴ the average number of silver atoms (N) per NC is calculated by using the following equation

$$N = \frac{0.5\pi N_A D^3}{3V} \quad (3)$$

where D is the mean particle diameter in nm, V is the molar volume of silver (10.5 mL mol^{-1}), and N_A is the Avogadro number. The estimation of the number of atoms in the NC using the above formula reveals an average number of 31 atoms on putting the value of $D = 1 \text{ nm}$ (obtained from TEM). On the other hand, putting the value of $N = 31$ in the formula for spherical jellium model,¹⁶ i.e., emission energy, $E = E_{\text{fermi}}/N^{1/3}$, gives the corresponding emission maximum to be around 700 nm, which is close to the experimentally observed emission maximum (680 nm) obtained from the CHT-conjugated Ag NCs (Figure 3). However, it has to be mentioned that the emission energies of clusters containing a greater number of atoms ($N > 20$) show some deviation from the jellium model due to the distortion of potential well used to describe the electronic transitions in these metal NCs.¹⁷ The electronic transition in these Ag NCs leading to luminescence is attributed to the recombination of the excited electrons from higher excited states in the sp band with the holes in the lower-lying d band (interband transition).

It is well-known that the sodium borohydride induces cleavage of disulfide bonds to sulfhydryl groups in a protein and perhaps breaks some of the peptide bonds also leading to its denaturation. Reconstitution of a protein denotes the process of returning of a denatured protein to its original structure and activity. Reconstitution of a reduced protein, without forming any kind of precipitation can be achieved easily, when oxidation is carried out at low protein concentrations and when conditions of surface denaturation (e.g., bubbling with air) are avoided.³⁵ Efficient oxidation occurs when dilute solutions, adjusted to pH 8.0–8.5, are allowed simply to stand in open vessels at room temperature for approximately 20 h yielding 80–100% reconstituted protein. In our experiment, CHT and Ag–CHT conjugates were reconstituted by dialyzing each of them separately against water of pH = 8.0–8.5 for 24 h in aerated conditions. Figure 4a compares the CD spectra of native CHT, reconstituted CHT, and reconstituted Ag–CHT solutions. Native CHT displays CD features with minima at 202 and 232 nm, corresponding to the native secondary and tertiary structure of the protein,^{36,37} respectively. As evident from Figure 4a, there is a slight loss of tertiary structure in the CD spectrum at 232 nm for the reconstituted CHT as well as reconstituted Ag–CHT samples compared to the native CHT. However, the overall structure of CHT was almost maintained as demonstrated by the minimal shift of the minimum at 202 nm³⁸ (Figure 4a) for the reconstituted CHT as well as reconstituted Ag–CHT compared to the native CHT. Quantification of the CD data through curve-fitting analysis revealed that the conformation of the reconstituted Ag–CHT (19% helix) was almost identical to that of the reconstituted CHT (18% helix), demonstrating a small perturbation of the native structure of the protein (24% helix).

We have also investigated the functionality of reconstituted enzyme and reconstituted Ag–CHT complex by measuring their enzymatic activity on a substrate AAF-AMC and recording the rate of formation of AMC–product as shown in Figure 4b. It has to be mentioned that the number of silver particles bound per enzyme is estimated from the number of atoms per Ag NC (~ 30) and the initial molar ratio of Ag atoms to chymotrypsin molecules (10:1) used in the preparation. This gives the estimation that one NC is attached to one enzyme from a random selection of three enzymes. Taken together, these facts imply

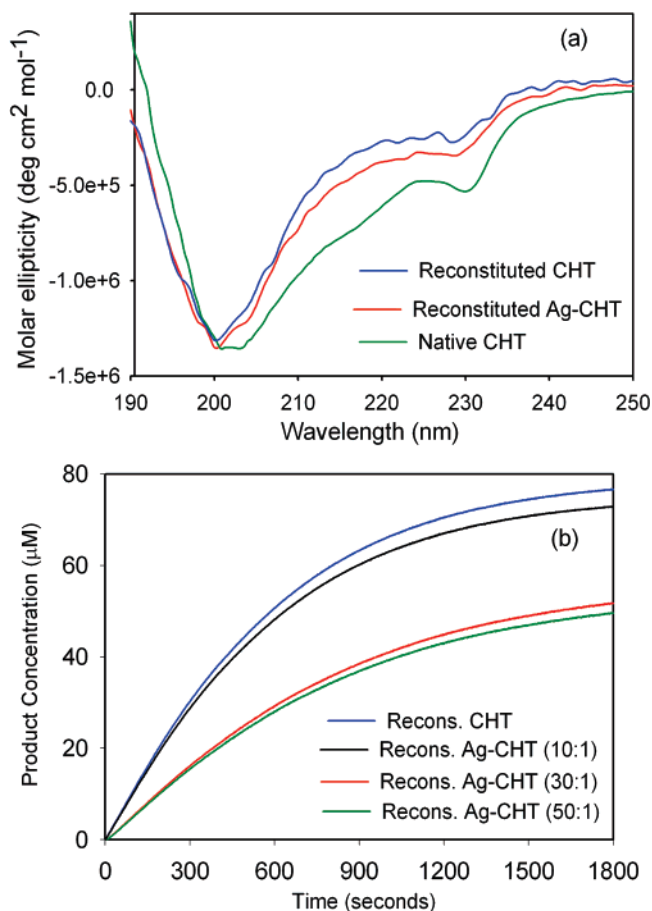


Figure 4. (a) CD spectra of native CHT, reconstituted CHT, and reconstituted Ag–CHT nanobioconjugates. (b) Enzymatic activities of reconstituted CHT and reconstituted Ag–CHT nanobioconjugates at molar ratios of 10:1, 30:1, and 50:1 (Ag:CHT) on the substrate, AAF-AMC.

TABLE 1: Comparison of Specific Activity in Units/mg of Native CHT with the Reconstituted CHT and Reconstituted Ag–CHT Nanobioconjugates^a

system	specific activity (units/mg)
native CHT	31
reconstituted CHT	11.5
reconstituted Ag–CHT (10:1)	10.9
reconstituted Ag–CHT (30:1)	5.7
reconstituted Ag–CHT (50:1)	5.5

^a One unit of CHT will hydrolyze 1.0 μmol of AAF-AMC per minute at pH 7.8 at 25 °C. It has to be noted that the vendor (Sigma-Aldrich) has reported the value of specific activity of the native CHT to be 40 units/mg using *n*-benzoyl-L-tyrosine ethyl ester as the substrate at pH 7.8 at 25 °C.

that many of the CHT molecules are free and may not be associated with Ag NC. Hence one may expect that there could be two subsets of protein complexes in the solution: one that is bound to Ag NC and another that includes all those that are enzymatically active. To prove that the Ag-bound CHT NCs are still functional, we also carried out the enzymatic activities of Ag–CHT having initial stoichiometries of Ag:CHT as 30:1 and 50:1 (Figure 4b). Table 1 lists the specific activity (in units/mg) of native CHT, reconstituted CHT, and reconstituted Ag–CHT nanobioconjugates. From Table 1, we find that the specific activity of the reconstituted Ag–CHT complex (Ag:CHT = 10:1) is close to the reconstituted CHT; however, compared to the native enzyme, it is retarded by ~ 2.8 times. On the other hand, at 30:1 (Ag:CHT) stoichiometry, where we expect all the CHT

to be completely complexed, the rate of enzymatic activity of the reconstituted Ag–CHT was found to be retarded by ~ 2 times compared to that of reconstituted CHT consistent with our previous studies³⁹ on an analogous system (CdS-bound CHT).

Our observation also closely matches with the enzymatic activities performed by Jordan et al.³⁷ for a similar system (CHT–Au–TCOOH; Au–TCOOH being the gold-nanoparticle-capped tetra(ethylene glycol) carboxylate ligands) where they observed a 3-fold decrease in the rate of CHT complexed with AuTCOOH compared to CHT alone. In another study⁴⁰ on the glutathione-mediated (GSH-mediated) reactivation of an enzyme, β -galactosidase bound to mixed monolayer protected clusters (MMPCs) of different chain lengths, 95% of the native enzymatic activity was rescued from MMPCs having shorter chain lengths at intracellular concentrations of GSH compared to MMPCs featuring longer chain lengths that did not display any reactivation for any concentrations of GSH used. Essentially similar specific activity of reconstituted Ag–CHT (Table 1 and Figure 4b) prepared using higher stoichiometry of Ag atoms to CHT molecules (Ag:CHT = 50:1) compared to the stoichiometry of 30:1 confirms that the Ag-bound CHT NCs are indeed functional. The above experimental observations may indicate that the nucleation and the subsequent growth of Ag NC in CHT could possibly take place at a site that is away from the enzymatic active site of CHT. It has to be noted that the attachment of 1 nm diameter NC to the active site of the enzyme is expected to act as an inhibitor of CHT activity on the substrate AAF-AMC (1–2 nm diameter) resulting in retardation of the enzymatic activity by several orders of magnitude.⁴¹ However, the moderate retardation in the enzymatic activity of Ag–CHT complex as compared to CHT alone could be the manifestation of the dynamical rigidity of CHT upon attachment of a Ag NC. It has to be mentioned here that the CD spectra of Ag–CHT complexes with higher stoichiometries of 30:1 and 50:1 (Ag:CHT) are similar to that of Ag–CHT complex with a lower stoichiometry of 10:1 (Ag:CHT). However, formation of some larger sized Ag clusters in Ag–CHT complex with higher Ag:CHT stoichiometries (30:1 and 50:1) was evidence from the absorption and emission spectra.

To confirm the conjugation of Ag NCs to CHT possibly via amines/thiols present in different residues, we carried out the FRET studies using a fluorescent probe, NPA, known to bind at the enzymatic active site⁴² of CHT as the donor and Ag NC bound CHT as the acceptor. The huge spectral overlap between NPA–CHT emission and the absorption of Ag–CHT NC is expected to reveal interprobe distance, when they are in a close proximity. Figure 5a reveals the significant spectral overlap between NPA–CHT emission spectrum (donor D, emission maximum at 428 nm) and Ag–CHT excitation spectrum (acceptor A, excitation maximum at 413 nm) that favors the energy transfer from NPA to Ag in CHT. It has to be noted that the absorption band of Ag–CHT bioconjugates remained the same even after the reconstitution process. The molar extinction coefficient of Ag–CHT conjugates required for energy transfer calculations was computed from theoretical considerations using the maximum absorbance value of the SPR band at 413 nm, the details of which are given in the Supporting Information. As revealed from Figure 5b the overall steady-state emission intensity of the donor emission drastically decreased in the presence of acceptor. Also, the faster decay of donor in the presence of acceptor (Figure 5c) as compared to that of the donor alone confirms the energy transfer from NPA to Ag cluster in CHT. The calculated (from eqs 4a and 4b) donor to acceptor energy transfer efficiency from steady-state and time-

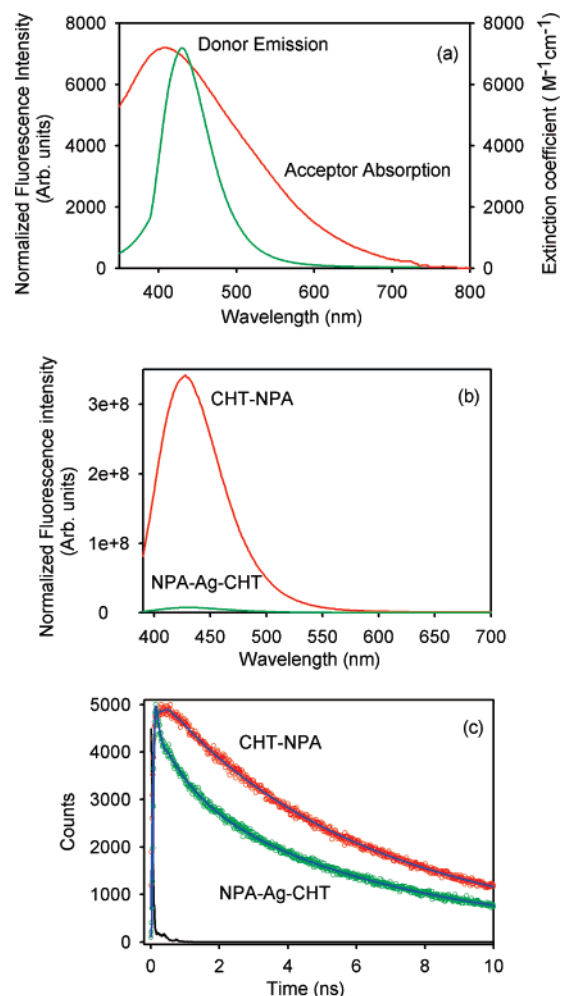


Figure 5. (a) Spectral overlap between the donor (NPA–CHT) emission and acceptor (Ag–CHT) absorption. (b) Steady-state PL quenching of NPA–CHT (donor) in the presence of acceptor (Ag–CHT nanobioconjugates). The optical density of the samples at excitation and emission wavelengths was 0.05 and 0.07, respectively. (c) Picosecond-resolved fluorescence transients of donor (NPA–CHT) and donor–acceptor (NPA–Ag–CHT) complex.

resolved studies are 97.5 and 60.7%, respectively. It has to be carefully noted that we have used the amplitude weighted time constants⁴³ for the donor in the absence ($\langle\tau_D\rangle$) and presence of acceptor ($\langle\tau_{DA}\rangle$) to evaluate the energy transfer efficiency (E) using time-resolved data (see Supporting Information for the details). The estimated donor–acceptor distances from steady-state and time-resolved experiments are 19.1 and 32.6 Å, respectively. For a well-behaved system, the ratio of the integrated areas under the time-resolved emission decays for donor and donor/acceptor complex should correlate with the integrated areas under the steady-state emission spectra. In principle, one of the methods can be used to estimate D–A distance. However, due to some possibility of reabsorption of donor emission by acceptor, there is a disagreement between the estimated donor–acceptor (DA) distances from steady-state and time-resolved studies. This is clearly evident from the comparison of parts b and c of Figure 5. Here we have used the time-resolved emission decays in order to estimate DA distances. In one of our recent studies,⁴⁴ we have reported the potential danger of using steady-state fluorescence quenching to conclude the nature of energy transfer as Förster type and to estimate the DA distances. The globular enzyme CHT has a diameter of 44 Å, and the estimated distance of any surface sites from the catalytic center is less than the diameter of the

enzyme. The possible nucleation sites (DA distance of 32.6 Å) for the formation of Ag NCs in CHT could be free amine groups from the amino acid residues or the thiols at the protein surface, which could have been easily generated by the reduction of disulfide bonds by NaBH₄.^{45,46} These functional groups (thiols and amines) have the ability to bind covalently with the silver particle surface, leading to the formation of nanobioconjugates.

Conclusion

We report the luminescence of Ag NCs (1 nm average diameter) directly conjugated to a macromolecular enzyme CHT. By use of the spherical jellium model, the emission energy of Ag NCs was correlated with the number of atoms in it and was found to be closely matching with the experimental result. The structural information of CHT before and after the conjugation of Ag NCs was obtained through circular dichroism (CD) spectroscopy. We found a small perturbation in the native structure of the protein in the reconstituted CHT as well as reconstituted Ag–CHT bioconjugates when compared to that of the pure CHT without reconstitution. The functional integrity of Ag–CHT bioconjugates was confirmed by monitoring the enzymatic activities of the reconstituted CHT and reconstituted Ag–CHT bioconjugates by using UV–vis absorption spectroscopy. The FRET studies using a fluorescent probe, NPA bound at the enzymatic active site of CHT, as the donor and Ag NC bound CHT as the acceptor confirmed the conjugation of Ag NCs to CHT. The unique properties of these luminescent NC bioconjugates may find their widespread applications in areas ranging from optoelectronics and biolabels to targeted therapeutic agents.

Acknowledgment. S.S.N. thanks CSIR, India for fellowship. We thank DST for financial grant (SR/FTP/PS-05/2004).

Supporting Information Available: The details of steady-state measurements, time-resolved measurements, DA distance measurements from FRET, and calculation of molar extinction coefficient of NC solutions from theoretical considerations are provided. This information is available free of charge via the Internet at <http://pubs.acs.org>.

References and Notes

- Niemeyer, C. M. *Angew. Chem., Int. Ed.* **2001**, *40*, 4128.
- Niemeyer, C. M. *Angew. Chem., Int. Ed.* **2003**, *42*, 5796.
- Murphy, C. J.; Gole, A. M.; Hunyadi, S. E.; Orendorff, C. J. *Inorg. Chem.* **2006**, *45*, 7544.
- Kamat, P. V. *J. Phys. Chem. B* **2002**, *106*, 7729.
- Ahmadi, T. S.; Wang, Z. L.; Green, T. C.; Henglein, A.; El-Sayed, M. A. *Science* **1996**, *272*, 1924.
- Andres, R. P.; Bein, T.; Dorogi, M.; Feng, S.; Henderson, J. I.; Kubiak, C. P.; Mahoney, W.; Osifchin, R. G.; Reifenger, R. *Science* **1996**, *272*, 1323.
- Galletto, P.; Brevet, P. F.; Girault, H. H.; Antoine, R.; Broyer, M. *J. Phys. Chem. B* **1999**, *103*, 8706.
- Mirkin, C. A.; Letsinger, R. L.; Mucic, R. C.; Storhoff, J. J. *Nature* **1996**, *382*, 607.
- Shenton, W.; Pum, D.; Sleytr, U. B.; Mann, S. *Nature* **1997**, *389*, 585.
- Braun, E.; Eichen, Y.; Sivan, U.; Ben-Yoseph, G. *Nature* **1998**, *391*, 775.
- Douglas, T.; Young, M. *Nature* **1998**, *393*, 152.
- Behrens, S.; Rahn, K.; Habicht, W.; Böhm, K.-J.; Rösner, H.; Dinjus, E.; Unger, E. *Adv. Mater.* **2002**, *14*, 1621.
- Mandal, S.; Phadtare, S.; Sastry, M. *Curr. App. Phys.* **2005**, *5*, 118.
- Lee, D.; Donkers, R. L.; Wang, G.; Harper, A. S.; Murray, R. W. *J. Am. Chem. Soc.* **2004**, *126*, 6193.
- Chen, S.; Ingram, R. S.; Hostetler, M. J.; Pietron, J. J.; Murray, R. W.; Schaaff, T. G.; Khoury, J. T.; Alvarez, M. M.; Whetten, R. L. *Science* **1998**, *280*, 2098.
- Zheng, J.; Zhang, C.; Dickson, R. M. *Phys. Rev. Lett.* **2004**, *93*, 077402.
- Zheng, J.; Nicovich, P. R.; Dickson, R. M. *Ann. Rev. Phys. Chem.* **2007**, *58*, 409.
- Wilcoxon, J. P.; Williamson, R. L.; Baughman, R. J. *Chem. Phys.* **1993**, *98*, 9933.
- Charle, K. P.; Schulze, W. *Ber. Bunsen–Ges. Phys. Chem.* **1984**, *88*, 350.
- Burt, J. L.; Gutiérrez-Wing, C.; Miki-Yoshida, M.; Jose'-Yacama'n, M. *Langmuir* **2004**, *20*, 11778.
- Zheng, J.; Stevenson, M. S.; Hikida, R. S.; Van Patten, P. G. *J. Phys. Chem. B* **2002**, *106*, 1252.
- Bley, R. A.; Kauzlarich, S. M. *J. Am. Chem. Soc.* **1996**, *118*, 12461.
- Henglein, A. *J. Phys. Chem.* **1993**, *97*, 5457.
- Mie, G. *Ann. Phys.* **1908**, *25*, 377.
- Doyle, W. T. *Phys. Rev.* **1958**, *111*, 1067.
- Zeman, E. J.; Schatz, G. C. *J. Phys. Chem.* **1987**, *91*, 634.
- Ghosh, B.; Chakraborty, P.; Mohapatra, S.; Kurian, P. A.; Vijayan, C.; Deshmukh, P. C.; Mazzoldi, P. *Mater. Lett.* **2007**, *61*, 4512.
- Balan, L.; Malval, J.-P.; Schneider, R.; Burget, D. *Mater. Chem. Phys.* **2007**, *104*, 417.
- Wilcoxon, J. P.; Martin, J. E.; Provencio, P. *J. Chem. Phys.* **2001**, *115*, 998.
- Kreibig, U.; Vollmer, M. *Optical Properties of Metal Clusters*; Springer: Berlin, 1995.
- Kreibig, U.; Genzel, L. *Surf. Sci.* **1985**, *156*, 678.
- Henglein, A.; Tausch-Treml, R. *J. Colloid. Interface Sci.* **1981**, *80*, 84.
- Vosch, T.; Antoku, Y.; Hsiang, J.-C.; Richards, C. I.; Gonzalez, J. I.; Dickson, R. M. *Proc. Natl. Acad. Sci. U.S.A.* **2007**, *104*, 12616.
- Henglein, A.; Giersig, M. *J. Phys. Chem. B* **1999**, *103*, 9533.
- Anfinsen, C. B.; Haber, E. *J. Biol. Chem.* **1961**, *236*, 1361.
- Hennessey, J. P.; Johnson, W. C. *Biochemistry* **1981**, *20*, 1085.
- Jordan, B. J.; Hong, R.; Gider, B.; Hill, J.; Emrick, T.; Rotello, V. M. *Soft Matter* **2006**, *2*, 558.
- Srivastava, S.; Verma, A.; Frankamp, B. L.; Rotello, V. M. *Adv. Mater.* **2005**, *17*, 617.
- Narayanan, S. S.; Sarkar, R.; Pal, S. K. *J. Phys. Chem. C* **2007**, *111*, 11539.
- Verma, A.; Simard, J. M.; Worrall, J. W. E.; Rotello, V. M. *J. Am. Chem. Soc.* **2004**, *126*, 13987.
- Béchet, J.-J.; Dupaix, A.; Yon, J.; Wakselman, M.; Robert, J.-C.; Vilkas, M. *Eur. J. Biochem.* **1973**, *35*, 527.
- Haugland, R. P.; Stryer, L. In *Conformation of Biopolymers*; Ramachandran, G. M., Ed.; Academic Press: New York, 1967; Vol. I, p 321.
- Lakowicz, J. R. *Principles of fluorescence spectroscopy*; Kluwer Academic/Plenum: New York, 1999.
- Majumder, P.; Sarkar, R.; Shaw, A. K.; Chakraborty, A.; Pal, S. K. *J. Colloid Interface Sci.* **2005**, *290*, 462.
- Gole, A.; Dash, C.; Ramakrishnan, V.; Sainkar, S. R.; Mandale, A. B.; Rao, M.; Sastry, M. *Langmuir* **2001**, *17*, 1674.
- Leff, D. V.; Brandt, L.; Heath, J. R. *Langmuir* **1996**, *12*, 4723.

Supporting Information

Structural and Functional Characterization of Luminescent Silver-Protein Nanobioconjugates

S. Shankara Narayanan and Samir Kumar Pal

*Unit for Nano Science & Technology,
Department of Chemical, Biological & Macromolecular Sciences,
S. N. Bose National Centre for Basic Sciences,
Block JD, Sector III, Salt Lake,
Kolkata 700 098, India*

1. Details of Steady-state and Time-resolved Measurements: Steady-state UV-vis absorption and photoluminescence (PL) were done using a Shimadzu UV-2450 spectrophotometer and a Jobin Yvon Fluoromax-3 fluorimeter, respectively. A JEOL JEM-2100 high-resolution transmission electron microscopy (HRTEM) equipped with an energy dispersive X-ray (EDAX) spectrometer was used to characterize the internal structures of samples and to analyze their elemental composition. Samples for TEM were prepared by placing a drop of the colloidal solution on a carbon-coated copper grid and allowing the film to evaporate overnight at room temperature. To obtain the clear TEM images of nanoclusters, the aqueous solution of Ag-CHT sample was dialyzed against Millipore water exhaustively using a dialysis membrane (Spectrum Laboratories, Inc, USA) with a molecular weight cut off (MWCO) of 12000-14000. The dialyzed solution was then placed on a separate carbon-coated copper grid and dried overnight at room temperature. We also obtained TEM images of the samples without dialysis. The size of the nanoparticles was determined from the TEM images obtained at 200 kV. The circular dichroism (CD) study was done using Jasco 815 spectropolarimeter using a quartz cell of path-length 10 mm. All of the

photoluminescence transients were taken using the picosecond-resolved time-correlated single photon counting (TCSPC) technique. We used a commercially available picosecond diode laser-pumped (LifeSpec-ps) time-resolved fluorescence spectrophotometer from Edinburgh Instruments, U.K. The picosecond excitation pulse from the picoquant diode laser was used at 375 nm with instrument response function (IRF) of 80 ps. A microchannel-plate-photomultiplier tube (MCP-PMT, Hamamatsu) was used to detect the photoluminescence from the sample after dispersion through a monochromator. For all transients the polarizer on the emission side was adjusted to be at 55° (Magic angle) with respect to the polarization axis of the excitation beam. The observed fluorescence transients were fitted by using a nonlinear least square fitting procedure to a function $(X(t) = \int_0^t E(t')R(t-t')dt')$

comprising of convolution of the IRF ($E(t)$) with a sum of exponentials ($R(t) = A + \sum_{i=1}^N B_i e^{-t/\tau_i}$) with preexponential factors (B_i), characteristic lifetimes (τ_i)

and a background (A). Relative concentration in a multiexponential decay is finally expressed as, $c_n = \frac{B_n}{\sum_{i=1}^N B_i} \times 100$.

To estimate the Förster resonance energy transfer efficiency of the donor (NPA-CHT complex) and hence to determine the distance of the donor–acceptor pair, we followed the methodology described in chapter 13 of reference¹. The Förster distance (R_0) is given by,

$$R_0 = 0.211[\kappa^2 n^{-4} Q_D J(\lambda)]^{1/6} \quad (\text{in } \text{Å}) \dots \dots \dots (1)$$

where κ^2 is a factor describing the relative orientation in space of the transition dipoles of the donor and acceptor. For donor and acceptors that randomize by

rotational diffusion prior to energy transfer, the magnitude of κ^2 is assumed to be 2/3. In the present study the same assumption has been made. The refractive index (n) of the medium is assumed to be 1.4. Q_D , the quantum yield of the donor QD in the absence of acceptor, is measured to be 0.51. $J(\lambda)$, the overlap integral, which expresses the degree of spectral overlap between the donor emission and the acceptor absorption, is given by,

$$J(\lambda) = \frac{\int_0^{\infty} F_D(\lambda) \varepsilon(\lambda) \lambda^4 d\lambda}{\int_0^{\infty} F_D(\lambda) d\lambda} \quad (2)$$

where $F_D(\lambda)$ is the fluorescence intensity of the donor in the wavelength range of λ to $\lambda+d\lambda$ and is dimensionless. $\varepsilon(\lambda)$ is the extinction coefficient (in $M^{-1} \text{ cm}^{-1}$) of the acceptor at λ . If λ is in nm, then $J(\lambda)$ is in units of $M^{-1} \text{ cm}^{-1} \text{ nm}^4$. Once the value of R_0 is known, the donor-acceptor distance (r) can easily be calculated using the formula,

$$r^6 = [R_0^6(1-E)]/E. \quad (3)$$

Here E is the efficiency of energy transfer. The transfer efficiency is measured by using the relative fluorescence intensity of the donor in the absence (F_D) and presence (F_{DA}) of the acceptor. The efficiency E is also calculated from the lifetimes under these respective conditions (τ_D and τ_{DA}).

$$E = 1-(F_{DA}/F_D), \quad (4a)$$

$$E = 1-(\tau_{DA}/\tau_D). \quad (4b)$$

The distances measured with eqs. 4a and 4b are revealed as R^S (steady-state measurement) and R^{TR} (time-resolved measurement), respectively.

It has to be noted that the equation 4b holds rigorously only for a homogeneous system (i.e. identical donor-acceptor complexes) in which the donor and the donor-acceptor complex have single exponential decays. However, for Donor-

Acceptor systems decaying with multiexponential lifetimes, Energy transfer efficiency (E) is calculated from the amplitude weighted lifetimes $\langle \tau \rangle = \sum_i \alpha_i \tau_i$ where α_i is the relative amplitude contribution to the lifetime τ_i ¹. We have used the amplitude weighted time constants for τ_D and τ_{DA} to evaluate the energy transfer efficiency (E) using Eq. 4b.

Catalytic activity measurements in our experiment were made using the substrate AAF-AMC. The extinction coefficient used for determining the concentration of AAF-AMC in buffer (10 mM, pH=7.0) is 16 mM⁻¹cm⁻¹ at 325 nm². For the kinetics experiment, the concentration of CHT and Ag-CHT was maintained at 10 μM, whereas that of substrate was maintained at 100 μM. The rate of formation of product was monitored by observing the change in the absorbance at 370 nm of the product with time. The product formed in the catalytic measurement was 7-amido-4-methyl coumarin (AMC) and its extinction coefficient at 370 nm is reported to be 7.6 mM⁻¹cm⁻¹.

2. Calculation of molar extinction coefficient of nanocluster solution (Ag-CHT) from theoretical considerations: Firstly, the molar concentration of the nanocluster solutions were calculated by dividing the total number of silver atoms (N_{total} , equivalent to the initial amount of silver salt added to the reaction solution) over the average number of silver atoms per nanocluster (N) determined from TEM, according to the equation³:

$$C = \frac{N_{total}}{NVN_A} \quad (5)$$

where V is the volume of the reaction solution in liter and N_A is the Avogadro's constant. It is assumed that the reduction from silver ions to silver atoms was 100% complete. The concentration of the diluted sample was then calculated from this

initial concentration. The extinction coefficient of the sample was then determined according to Lambert–Beer law, Eq. 6 by measuring the absorbance at 413 nm (SPR peak of silver nanocluster solution).

$$A=\epsilon Cl \quad (6)$$

The molar extinction value obtained at SPR peak is $8153 \text{ M}^{-1}\text{cm}^{-1}$.

References:

- (1) Lakowicz, J. R. *Principles of fluorescence spectroscopy*; Kluwer Academic/Plenum: New York, 1999.
- (2) Kamal, J. K. A.; Xia, T.; Pal, S. K.; Zhao, L.; Zewail, A. H. *Chem. Phys. Lett.* **2004**, 387, 209.
- (3) Liu, X.; M., A.; Wang, J.; Huo, Q. *Colloids and surfaces B* **2007**, 58, 3.